

# Velocities and concentrations in oscillatory flow over beds of sediment

By J. E. DICK AND J. F. A. SLEATH

Department of Engineering, University of Cambridge, Trumpington Street,  
Cambridge CB2 1PZ, UK

(Received 15 November 1989 and in revised form 16 May 1991)

Measurements are reported of the velocity and concentration distributions both within and above two beds of sediment in oscillatory flow. The experiments were carried out in an oscillatory flow water tunnel, the velocities were measured with a laser-Doppler anemometer and the concentrations of sediment with resistance probes operating through the sidewall of the tunnel. The sediments studied consisted of nylon granules of median diameter 4.0 mm and Perspex of median diameter 0.7 mm. Most of the beds were plane for the tests with the 0.7 mm sediment and rippled for those with the 4 mm sediment.

The measured velocity profile could be divided into three regions: a central region in which the amplitude and phase of the velocity increased almost linearly with height and two outer regions in which the variation in velocity with height was much less rapid. It is suggested that at very high sediment transport rates the central region covers almost the entire depth of the moving bed but that at lower transport rates the outer regions are more significant.

The effect of sediment movement on the velocity distribution above the bed is very marked. Bed roughness length is increased and the velocity amplitude falls off more slowly with height than for fixed beds under similar conditions.

Within the bed the shear stress increases almost linearly with depth. Apparent viscosity also increases steadily with depth below the surface of the bed.

The measurements of concentrations are in good agreement with the results of other investigators in the region above the moving bed. Within the bed the time-mean concentration rises steadily, with distance below the initial bed surface, towards the limiting value for a stationary bed. The concentration record also shows a fluctuation during the course of the cycle at twice the frequency of the fundamental oscillation. The amplitude of this fluctuation in concentration decreases with depth below the initial bed level. The phase variation with height is close to that of zero velocity gradient, within the moving bed.

---

## 1. Introduction

The way in which sediment is moved around by the sea is of considerable importance but we are still a long way from being able to predict sediment transport in most situations of interest. One of the main difficulties concerns the calculation of flows with high concentrations of sediment. There have been many studies, both theoretical and experimental, of fluid/sediment interactions at very low sediment concentrations and significant progress has been made in this area. In comparison, the behaviour of fluid/sediment mixtures at high concentrations is poorly

understood. This is particularly true of oscillatory flows which is the subject of the present paper.

Measurements of bed-load in oscillatory flow have been made with sediment traps by Manohar (1955), Kalkanis (1964) and Abou-Seida (1965) but these give no information on the way in which the sediment transport varies during the course of the wave cycle. More recently, Sleath (1978) made optical measurements at low sediment transport rates, Horikawa, Watanabe & Katori (1982) and Sawamoto & Yamashita (1986) studied sheet flow in sand and Ahilan & Sleath (1987) observed velocity distributions within moving beds at high transport rates. However, each of these investigations covers only a restricted experimental range. There is no equivalent in oscillatory flow of the major experimental studies of Bagnold (1954), Savage & McKeown (1983), Hanes & Inman (1985) of fluid/sediment interactions in steady flows.

There have also been a number of analytical studies of this problem. Abou-Seida (1965) extended the steady-flow model of Einstein (1950) to oscillatory flow. More recently, Ahilan & Sleath (1987) put forward an oscillatory flow model using the steady-flow relations obtained by Bagnold (1954) and Savage & McKeown (1983). Neither of these models provides good agreement with experimental data. Sleath (1978) showed that some of the key assumptions in Abou-Seida's model were not valid for oscillatory flow. It may be that other assumptions in both models are invalid but there is too little data, at the present time, to be sure of this.

The aim of this paper is to provide additional oscillatory flow data which may be used to test existing assumptions and to form a basis for new models. There is a particular need for velocity measurements with relatively fine sediment. Both Ahilan & Sleath (1987) and Sawamoto & Yamashita (1986) measured velocity distributions but Ahilan & Sleath only tested very coarse sediment and Sawamoto & Yamashita only studied rather thin mobile bed layers so it is difficult to obtain much detail from their tests. There is also a need for simultaneous concentration measurements to allow the testing of the steady flow results of Bagnold (1954) and others.

## **2. Experimental apparatus**

The measurements were made in the oscillatory flow water tunnel described by Du Toit & Sleath (1981). This water tunnel consists essentially of a U-tube of rectangular cross-section. One arm of the U-tube is open to the atmosphere but the other contains a paddle driven through a crank by a variable speed motor with feedback control. The horizontal working section of the tunnel is approximately 3.7 m long, 0.31 m wide and 0.45 m high. The only significant addition to the tunnel in the present tests was the installation of grooved rubber matting on the floor of the tunnel to prevent slipping of the sediment. The grooves had a wavelength of 3 mm and height equal to 2 mm.

The sediment was usually installed in the working section to a depth of about 0.14 m. Two different sediments were used. One consisted of ICI Diakon acrylic granules of density  $1141 \text{ kg/m}^3$  and median diameter 0.7 mm. The other was ICI Maranyl nylon pellets of density  $1137 \text{ kg/m}^3$  and median diameter 4.0 mm. Figure 1 shows particle size distributions. The nylon pellets which were approximately cylindrical in shape were the same as those investigated by Ahilan & Sleath (1987). The acrylic particles were subspherical in shape. These very light particles of sediment were chosen in order to provide a moving layer of sediment as thick as possible. Very much higher free-stream velocities would have been required to obtain



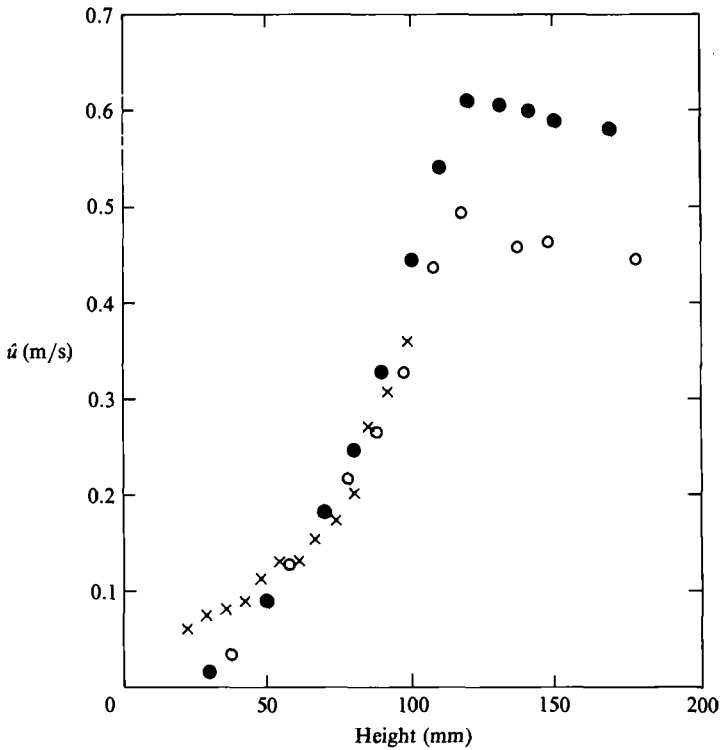


FIGURE 2. Comparison of measurements of grain velocity made by Ahilan (1985) with the present measurements of fluid velocity: ●, test 29; ○, test 31; x, Ahilan.

signal during the time that a grain of sediment is crossing the measuring volume. It follows from this that the velocity recorded by the tracker is essentially that of the fluid (if one accepts that the Mearlmaid particles move with the fluid). It is of interest to consider whether this is the same as that of the particles of sediment. The question of slippage between grains of sand and the fluid has been extensively discussed by Nielsen (1984). He concluded that under the conditions normally encountered in wave-induced flows the difference between the horizontal velocity of the sand and that of the water is negligible. This would be even more true in the present case because the density of our sediments is so close to that of water. However, Nielsen's calculations were limited to low sediment concentrations. At high sediment concentrations we may estimate the slippage to be of the same order of magnitude as the seepage velocity in the permeable bed. An estimate of this seepage velocity may be obtained with the aid of the formula for permeability proposed by Krumbein & Monk (1942). For the 4 mm sediment at a period of 4.5 s the calculated value of  $\hat{u}/U_0$  due to seepage is approximately 0.008, where  $\hat{u}$  and  $U_0$  are, respectively, the amplitude of the fluid velocity in the bed and in the free stream above the bed. This value of  $\hat{u}/U_0$  is negligible compared with the measured values given below. Since permeability is approximately proportional to the square of the grain diameter the seepage velocities for the 0.7 mm sediment would be even smaller.

A second, somewhat less conclusive, check on the question of fluid/grain slippage is provided by comparison of the present results with those of Ahilan (1985) who measured grain velocities directly. Figure 2 shows the velocity amplitude for the present tests 29 and 31 together with Ahilan's results for his test no. 4 which was intermediate in period and free-stream velocity between these two tests but involved

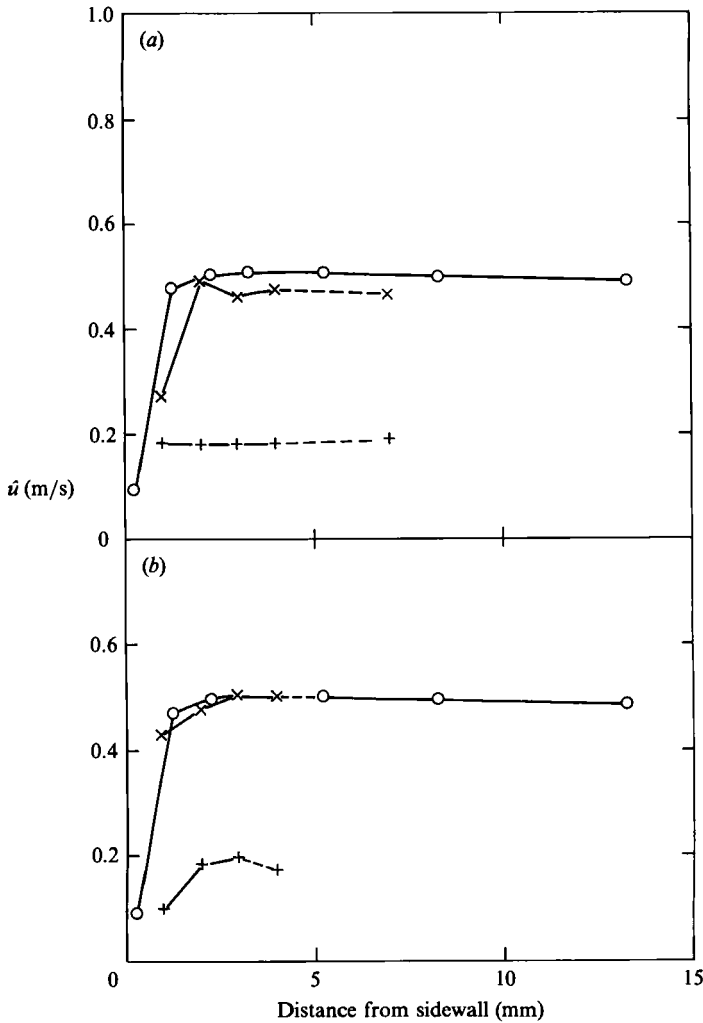


FIGURE 3. Variation of velocity amplitude with distance from tunnel sidewall. (a)  $D = 0.7$  mm:  $\circ$ ,  $y = 200$  mm;  $\times$ ,  $y = 0.8$  mm;  $+$ ,  $y = -22$  mm; (b)  $D = 4.0$  mm:  $\circ$ ,  $y = 200$  mm;  $\times$ ,  $y = 17$  mm;  $+$ ,  $y = -3$  mm.

the same 4 mm sediment. Only Ahilan's cross-correlation results are shown because the cine-film measurements were inherently less accurate. We see close agreement between the present measurements and those of Ahilan except at very low velocities. The most likely explanation for the discrepancy at low velocity is the inability of the cross-correlation device to distinguish between separate grains rocking in front of the two viewing apertures and a single grain passing first in front of one aperture and then in front of the other.

Since the velocity distribution is measured through the sidewall of the tunnel, it is necessary to consider the possible influence of the wall boundary layer on the measurements.

Figure 3 shows measurements of the amplitude of the velocity  $\hat{u}$  at various distances from the sidewall for two tests (one with each sediment). In this figure,  $y$  is height measured up from the initial bed surface level. Thus in figure 3(a) the profile at  $y = 200$  mm is well up in the clear fluid whereas the profile at  $y = -22$  mm is in

a region of high sediment concentration. In figure 3(b) both the  $y = 200$  mm and the  $y = 17$  mm profiles are for virtually clear fluid whereas at  $y = -3$  mm the sediment concentration is high throughout the cycle. The clear fluid profiles are in close agreement with Stokes' (1851) solution for oscillatory flow over a plane wall. The theoretical profile is not shown in the figure in order to avoid confusion.

These traverses show that velocity measurements can be made at surprisingly large distances into the bed even at very high sediment concentrations. This is because the laser beams can pass on either side of a given particle of sediment as well as in the gaps between particles. Of course, the signal becomes progressively more intermittent as distance from the sidewall increases. This is why the velocity profiles are shown as broken curves beyond about 3–4 mm from the wall in the high concentration regions. In view of these results it was decided, for the main body of tests, to make velocity measurements within the high-concentration region at 3 mm from the sidewall and within the low-concentration region at 10 mm from the sidewall. In the intermediate region, velocities were measured at both 3 mm and 10 mm and which measurement to adopt was subsequently decided by examination of the degree of intermittency of the records.

The only calibration of the laser-Doppler anemometer which was necessary was of the frequency tracker. This was carried out by supplying signals of known frequency from a signal generator and then monitoring computer output.

#### **4. Measurement of the sediment concentration**

The concentration of sediment was measured with single electrode conductivity probes. Since both of the sediments used in these experiments are good insulators, measurement of the local resistance of the fluid/sediment mixture gives an indication of the concentration. Fifteen probes were inserted through the wall of the tunnel at various heights above and below the initial bed level. Each probe was constructed of stainless steel wire of diameter 0.5 mm. Previous investigators (Gibson & Schwarz 1963; Chua, Cleaver & Millward 1986) have recommended the use of platinum wire. However, under the present test conditions, preliminary experiments with platinum wire showed no significant advantage over stainless steel. Polarization of the electrodes was minimized by connecting them to an a.c. bridge with 5 kHz supply.

A first point which needs to be considered is the size of the measuring volume of each probe in comparison to the concentration gradient of the fluid/sediment mixture. According to Gibson & Schwarz (1963), the effective measuring radius of each probe is ten times the electrode radius, i.e. 2.5 mm in the present case. Here 'effective radius' is the radius of the sphere whose resistance from centre to outer surface is 90% of the resistance between the probe and infinity. However, because the contribution to the measured resistance falls off exponentially with radius most of the resistance is provided by a significantly smaller volume. Since the minimum thickness of the moving layer of sediment in these tests was at least 30 mm the discrimination of concentration gradient should be adequate.

The end of each probe on the inside of the tunnel was filed flush with the wall. This was done in order to avoid disturbance of the flow by the probes. At first sight it might seem that the measurements would be influenced by the non-uniform concentration adjacent to the wall. However, this does not necessarily mean that the probes will function incorrectly. It is probable that there is a unique relationship between the concentration of sediment in the wall layer and that in the interior of the fluid. If that is the case, the mean concentration of sediment in the probe

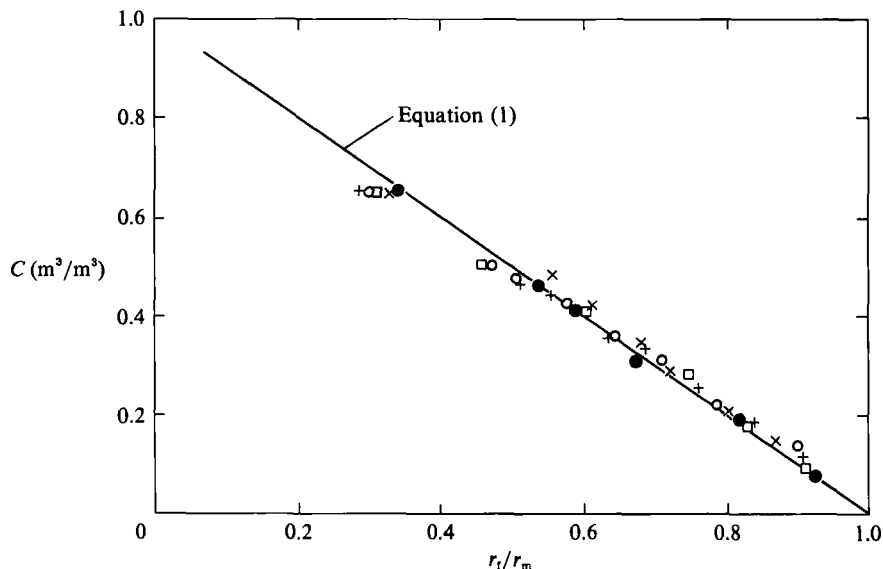


FIGURE 4. Typical calibration curve (measurements made on five separate days).

measuring volume will be monotonically related to the concentration in the interior of the fluid and, consequently, it will be possible to obtain a unique calibration curve linking the mean concentration of sediment outside the wall layer to the resistance measured by the probe.

The concentration probe was calibrated in a specially constructed container. One wall carried a pair of electrodes with a tap between them to allow sampling of the fluid-sediment mixture. The container was initially filled with clean water and then sediment was added through a hole in the top. The particles of sediment were maintained in suspension by a propeller driven by an electric motor. Figure 4 shows typical calibration curves for the 0.7 mm sediment.

The straight line in figure 4 corresponds to

$$\frac{r_t}{r_m} = 1 - C, \tag{1}$$

where  $r_t$  is the resistivity of the clear fluid,  $r_m$  that of the fluid-sediment mixture and  $C$  the volume concentration of the sediment. This equation is similar in form to the theoretical expression derived by Landauer (1952), in the limit as sediment conductivity tends to zero.

The measurements in figure 4 were made on five separate days. The fact that there is a well-defined curve linking mean concentration in the container to measured probe resistance and that the curves obtained on different days are so nearly identical appears to confirm that the probes can be expected to give a reliable indication of the concentration of sediment beyond the layer immediately adjacent to the wall.

The measurements in figure 4 are for the 0.7 mm sediment. The calibration measurements for the 4.0 mm sediment were much less consistent. There are two possible reasons for this. Firstly, the fluctuations in resistance as individual grains of sediment are swept past the probe are much larger. This makes determination of the mean resistance  $r_m$  less certain. Secondly, the thickness of the wall layer, in which concentration is different to that in the interior of the fluid, is proportional to grain

size. Consequently the wall layer is much thicker compared with the measuring volume of the probes for the 4.0 mm sediment than for the 0.7 mm sediment. Because of this only the concentration measurements for the 0.7 mm sediment will be presented below.

Finally, it should be mentioned that the experiments were carried out with ordinary tap water whereas most investigations with this sort of probe make use of salt water to reduce the resistivity. Although the use of tap water requires greater stability and sensitivity from the measuring instrument, it is clear from the calibration curves in figure 4 that the resistivity of the water was not too high for reliable measurement of the sediment concentration.

Further details of the experimental apparatus and methods are given by Dick (1989). It should, however, be mentioned that some of the results presented in that dissertation have subsequently been re-analysed.

## 5. Dimensionless groups

The independent variables relevant to this problem are:

$$\rho, \rho_s, g, \nu, D, U_0, a, y,$$

where  $\rho$  is the density of the fluid,  $\rho_s$  that of the water,  $g$  is the acceleration due to gravity,  $\nu$  is kinematic viscosity,  $D$  is median grain size,  $U_0$  is the amplitude of the velocity outside the boundary layer,  $a$  is the orbital amplitude of the fluid outside the boundary layer and  $y$  is the height above the bed. Bearing in mind that  $\rho_s$  and  $g$  combine with  $\rho$  in a buoyancy term we have four independent dimensionless groups. These may be expressed in various forms but the following are typical:

$$\frac{\rho U_0^2}{(\rho - \rho_s) g D}, \quad \frac{U_0 D}{\nu}, \quad \frac{a}{D}, \quad \frac{y}{D}.$$

Another dimensionless group which is frequently found to be important in problems involving sediment transport is the Shields parameter which expresses the ratio of the shear force on the bed to the immersed weight of sediment. However, since the shear stress on the bed is a function of  $a/D$  and  $U_0 D/\nu$ , this parameter is not independent of the four groups listed above. Similarly, the square of the ratio of grain size to viscous boundary-layer lengthscale  $D^2/\nu T$  is equal to  $(U_0 D/\nu)/(2\pi a/D)$ . Here  $T = 2\pi a/U_0$  is the period of oscillation.

It would clearly require an immense amount of data to define all four dimensionless groups individually. Consequently, previous investigators have tended to concentrate on one or other of these groups, or some combination of them. Since we, too, have only limited data we will follow previous practice and concentrate our discussion on those groups which other investigators have found to be most significant. Unfortunately, what appears to be important in one context is not necessarily important in another. It seems not to be possible to pick a single dimensionless group which is relevant in all cases.

## 6. Test conditions

Table 1 shows the experimental conditions for these tests. In this table  $\hat{u}_*$  is the friction velocity

$$\hat{u}_* = (\hat{\tau}_0/\rho)^{\frac{1}{2}}, \quad (2)$$

where  $\hat{\tau}_0$  is the amplitude of the shear stress. The value of  $\hat{u}_*$  quoted in table 1 is based on the shear stress calculated from the momentum integral for the initial bed

Test no.	$T$ (s)	$U_0$ (m/s)	$\nu \times 10^6$ (m <sup>2</sup> /s)	$a/D$	$\delta_s$ (mm)	$\delta_m$ (mm)	$\hat{u}_*$ (m/s)	$\delta_c$ (mm)	$1/K_1 D$ (mm)	$k_s/D$	Symbol
Diakon ( $D = 0.7$ mm)											
5	4.52	0.612	1.12	628.9	87	99	0.0689	91.0	88.1	32.3	+
6	4.50	0.539	1.07	551.5	58.3	61	0.0734	57.8	81.6	64.1	●
7	4.53	0.472	1.06	486.1	36.3	27	0.0649	36.1	36.6	49.6	✱
10	4.50	0.534	1.04	546.4	52.3	36	0.0566	52.0	41.3	30.7	✱
11	4.40	0.546	1.03	546.2	66.3	55	0.0484	66.3	61.6	28.4	▽
12	4.04	0.652	1.03	598.9	84.3	85	0.0807	82.3	86.0	110.4	△
13	4.50	0.671	1.07	686.5	88.3	92	0.0730	95.2	112.4	118.9	◇
14	4.50	0.727	1.04	743.8	116.4	110	0.0875	115.9	141.4	65.3	○
15	4.50	0.846	0.99	865.6	116.4	118	0.0779	115.4	187.0	22.8	⊗
16	4.40	0.867	1.01	867.3	114.4	115	0.0799	112.1	188.4	27.4	⊕
17	3.80	0.805	1.01	695.5	115.4	111	0.0679	114.5	171.1	9.87	×
18	4.40	0.370	1.01	370.1	30.4	19	0.0285	30.2	36.9	3.57	⊕
19	2.50	0.301	1.17	171.1	35.2	25	0.0263	34.9	40.3	4.53	⊗
20	2.70	0.563	1.08	345.6	103.2	101	0.0445	105.7	140.0	4.43	⊕
21	2.70	0.447	1.07	274.4	95.2	96	0.0491	94.5	77.3	14.5	▲
23	2.75	0.536	1.03	335.1	113.2	115	0.0464	115.7	130.0	7.74	▼
24	2.47	0.381	1.11	214.0	79.2	80	0.0470	79.0	—	18.8	◆
Maranyl ( $D = 4.0$ mm)											
26	4.35	0.782	1.10	135.3	82	85	0.1138	—	27.9	24.4	■
28	4.54	0.390	1.11	70.5	50	40	0.0706	—	9.83	27.8	●
29	4.60	0.578	1.11	105.8	87	86	0.0937	—	16.0	22.8	✱
30	2.70	0.539	1.08	57.9	87	92	0.0683	—	21.4	7.21	✱
31	2.60	0.445	1.07	46.0	87	87	0.0619	—	22.1	9.17	▽
32	2.56	0.277	1.04	28.2	79	72	0.0462	—	6.68	8.83	◆
33	2.60	0.543	1.03	56.2	87	82	0.0473	—	20.3	0.94	■
34	4.47	0.727	1.03	129.3	87	80	0.1060	—	28.1	21.9	●

TABLE 1. Test conditions

level. The quantities  $\delta_s$ ,  $\delta_c$  and  $\delta_m$  are defined in §7 and  $k_s$  is the bed roughness length determined from the velocity profile.

One of the original aims of this work was to study velocities and concentrations at high sediment transport rates. Consequently, many of the tests are in or near the sheet flow regime. Figure 5 shows how the test conditions compare with the limits for sheet flow suggested by Manohar (1955) and Dingler & Inman (1976). Visual observations of the bed during these tests were in reasonable agreement with the suggested limits. All of the tests with the 0.7 mm sediment appeared to be in the sheet flow or transition to sheet flow regime whereas the 4.0 mm sediment tests were mainly in the ripple or transition regime. Clearly, the transition from one regime to another is gradual so classification is subjective.

The ensemble average velocities and concentrations presented below are based on 100 cycles in each case.

### 7. Thickness of moving bed layer

The quantities  $\delta_s$  and  $\delta_m$  in table 1 refer to the thickness of the moving bed layer as defined in figure 6. The initial bed height is that measured in still fluid before the start of each test. Thus  $\delta_s$  multiplied by the concentration of sediment in a stationary bed provides a measure of the total quantity of sediment in motion. In most of the present tests there was a fairly sharp transition between the mass of sediment

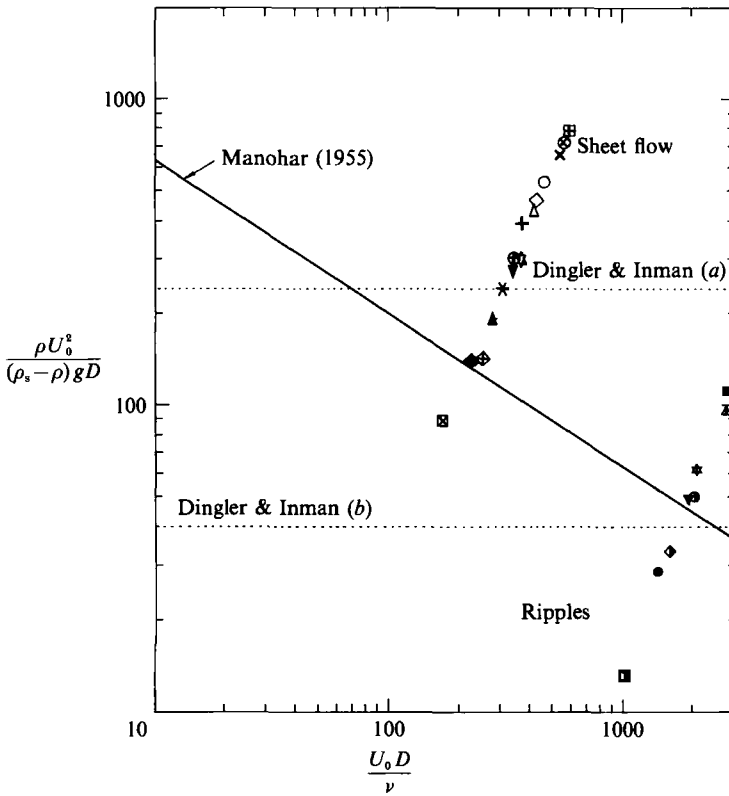


FIGURE 5. Bed regimes. Symbols shown in table 1. The dotted lines labelled Dingler & Inman are: (a) boundary between sheet flow and transition ripples; (b) boundary between transition ripples and vortex ripples.

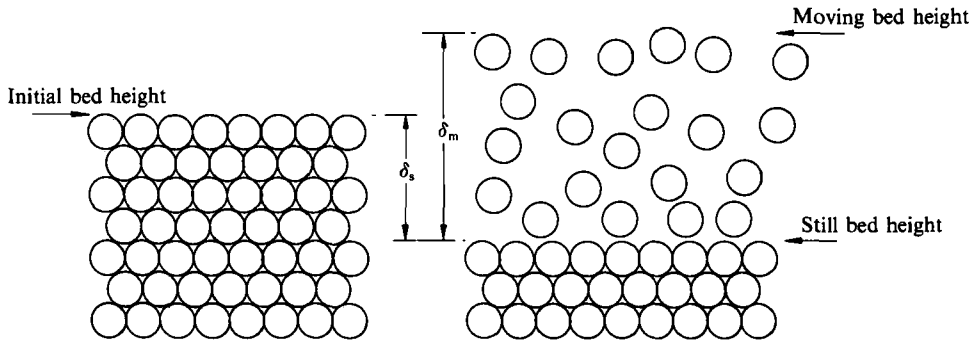


FIGURE 6. Definition sketch for  $\delta_s$ ,  $\delta_m$  and bed levels.

moving as bed load and the relatively clear fluid above. However, the height of this transition above the floor of the tunnel varied during the course of the cycle. For present purposes the minimum value of this height is designated as the moving bed height. The decision as to where to take this height was, inevitably, subjective. This is why the values of  $\delta_m$  in table 1 are sometimes smaller than  $\delta_s$  and sometimes larger. Finally, the still bed height is the highest level above the floor of the tunnel for which there was no observable motion of the sediment at any instant in the cycle of oscillation. In the present tests there was always at least 5 mm of stationary sediment below this level.

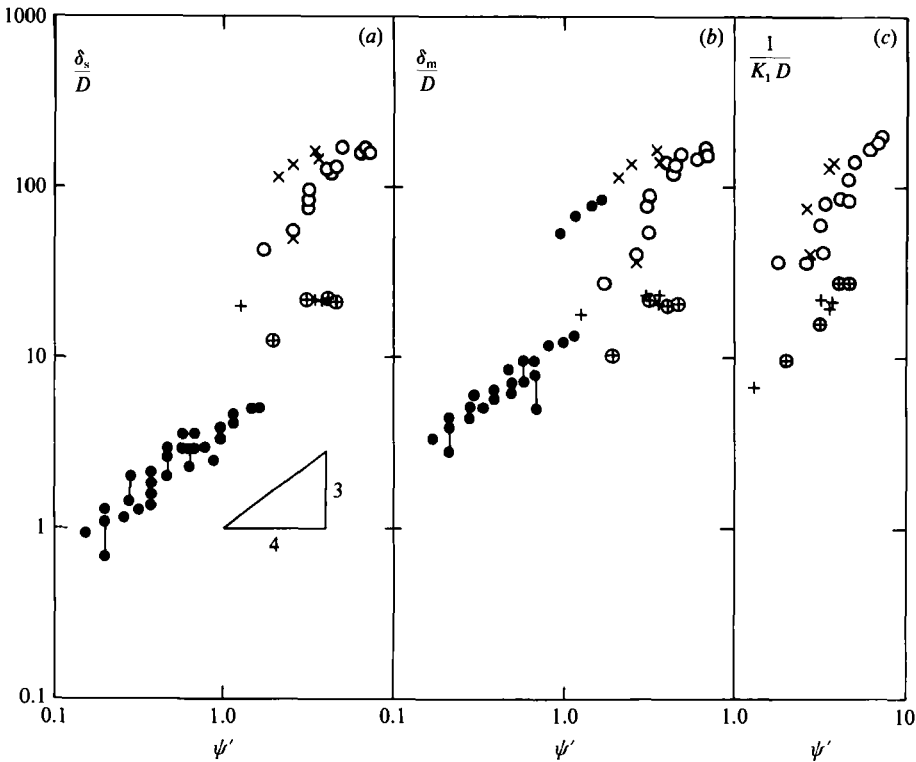


FIGURE 7. Variation of mobile bed thickness with Shields parameter; (a)  $\delta_s/D$ , (b)  $\delta_m/D$ , (c)  $1/K_1 D$ .  $\circ$ , tests 5-18;  $\times$ , tests 19-24;  $\oplus$ , tests 26-29, 34;  $+$ , tests 30-33;  $\bullet$ , Sawamoto & Yamashita (1986).

Figure 7 shows how  $\delta_s$  and  $\delta_m$  vary with the Shields parameter

$$\psi' = \frac{\hat{\tau}_{01}}{(\rho_s - \rho)gD}, \tag{3}$$

where  $\hat{\tau}_{01}$  is the amplitude of the shear stress calculated using Jonsson's (1963) curve for a fixed rough bed. The measurements of Sawamoto & Yamashita (1986) are also shown in this figure. Sawamoto & Yamashita suggested that both  $\delta_s/D$  and  $\delta_m/D$  were proportional to  $\psi'$  to the power  $\frac{3}{4}$ . It would seem from the present results that while this may be true at low values of  $\psi'$  the rate of increase of  $\delta_s$  and  $\delta_m$  with  $\psi'$  is significantly greater at high values of  $\psi'$ .

Since measurements have been made of the velocity and concentration distributions it would be possible to define the moving-bed thickness in terms of either velocity or concentration. For example, we see in §8.1 that the velocity profile is linear over almost the whole depth of the moving bed. The length  $1/K_1$  could be adopted as a measure of moving-bed thickness, where  $K_1$  is the gradient of the linear section of the velocity profile divided by the amplitude of the free-stream velocity. Values of  $K_1$  have been determined for each test using a least-squares technique and are listed in table 1. Figure 7(c) shows  $1/K_1 D$  plotted against Shields parameter. Although there is some reduction in experimental scatter compared with the direct visual observations of  $\delta_s$  shown in figure 7(a) it would seem that other dimensionless groups apart from  $\psi'$  may be important or that the moving-layer thickness does not scale with  $D$ .

An alternative would be to define moving-bed thickness in terms of sediment concentration  $C$ . The most obvious approach would be to define a thickness corresponding to a certain percentage of the sediment in the moving layer. However, this is rather a laborious procedure and relies on highly accurate measurements of concentration throughout the moving layer and throughout the cycle. A more direct approach is to define the upper boundary of the moving-bed layer as the point where sediment concentration falls to some specified value. In the measurements with the 0.7 mm sediment the mean value for all tests of the cycle-mean concentration  $\bar{C}$  at the initial bed level was  $0.22 \text{ m}^3/\text{m}^3$ . This is 34 % of the limiting concentration  $C_*$  for a stationary bed of this sediment. If we take the upper edge of the moving layer as the point where  $\bar{C}$  is equal to  $0.22 \text{ m}^3/\text{m}^3$  we obtain revised values for bed-layer thickness, denoted by  $\delta_c$ , which are shown in table 1. We see that the difference between  $\delta_c$  and  $\delta_s$  is small. Values of  $\delta_c$  are not shown for the 4.0 mm sediment because of the uncertainties about concentration measurement with this sediment outlined in §4.

## 8. Velocity measurements

The velocity distribution shows very different trends depending on whether the measurements are within the moving bed or in the relatively clear fluid above.

### 8.1. Velocity measurements within the moving bed

Figure 8 shows how the amplitude of the horizontal velocity  $\hat{u}$  varies with height for four tests with the 0.7 mm sediment. We see that in these tests the variation of velocity amplitude with height is approximately linear over almost the entire depth of moving bed. In addition to the linear region, the velocity profile shows transition regions, to zero velocity at the still bed level and to the free-stream velocity at the surface of the bed. The velocity distribution for the 4 mm sediment is similar to this except that the region in which the velocity profile is approximately linear is usually less extensive than in figure 8, particularly for the tests with the shortest periods.

The horizontal axis in figure 8 has been scaled in terms of the coefficient  $K_1$  defined in §7. Since most of the variation in velocity occurs within the moving bed it is to be expected that  $1/K_1$  would correlate with the thickness of the moving bed. Figure 9(a) shows how  $1/K_1$  varies with  $\delta_s$ . We see that at high sediment transport rates (large  $\delta_s$ )  $1/K_1$  is approximately equal to  $\delta_s$  but that under less severe flow conditions  $1/K_1$  is less than  $\delta_s$ . This is what we would expect since  $1/K_1$  is a measure of the thickness of the steeply rising portion of the velocity profile in figure 8 whereas  $\delta_s$  includes also the region at very low velocity where variation of velocity with height is small. At high sediment transport rates the thickness of this region of slowly varying velocity is small compared with the overall thickness of the moving bed but at low transport rates it is relatively more important.

Figure 9(a) also shows values of  $K_1$  for Ahilan's (1985) measurements with the same 4 mm sediment using a cross-correlation device. Because of doubts about the reliability of this device at low particle speeds only velocities greater than 0.1 m/s are included in the least-squares determination of  $K_1$ . The values of  $\delta_s$  for these tests may also be unreliable since Ahilan only records the 'moving-bed thickness' which is probably not quite the same as  $\delta_s$ . Bearing in mind these uncertainties, the agreement between the two sets of measurements is acceptable.

The origin for  $y$  in figure 8 is the initial bed level. This height has the advantage that it is easily identified experimentally. In the present tests the mean bed level did

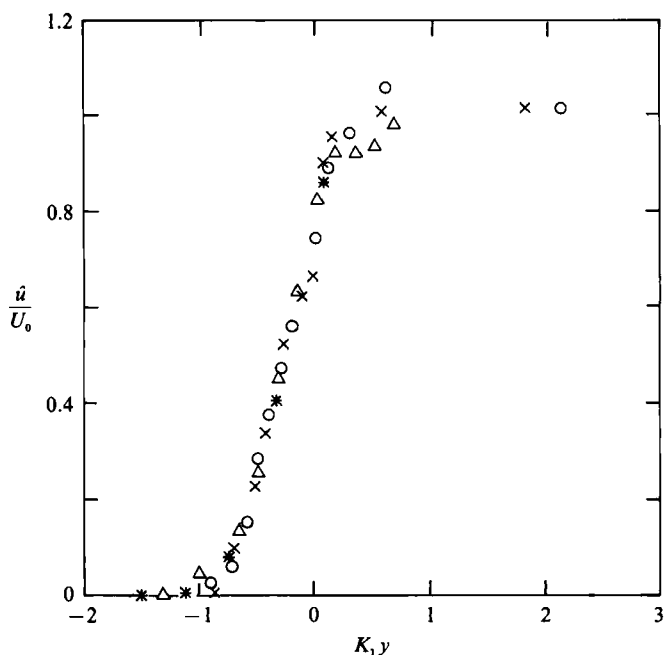


FIGURE 8. Variation of horizontal velocity amplitude with height. Symbols shown in table 1.

not change significantly during the course of a test. This is not always the case, particularly where there is also a steady current. In these situations it might be preferable to identify an origin directly from the velocity profile; for example, the point where the least squares line through the steeply rising portion of the velocity profile intersects the  $\hat{u} = 0$  axis. Figure 9(b) shows how the distance  $Y$  between this point and the initial bed level ( $y = 0$ ) varies with  $\delta_s$ . In the same way as for  $1/K_1$ , we see that  $Y$  is less than  $\delta_s$  at small transport rates but tends to approach  $\delta_s$  as sediment transport rate increases. Ahilan (1985) does not provide sufficient information to allow values of  $Y$  to be determined for his results.

The variation in phase with height also appears to be approximately linear in the moving-bed layer as shown by figure 10. The origin of  $y$  and the scaling parameter  $K_1$  are the same as for figure 8. The experimental scatter is somewhat reduced if a scaling parameter  $K_2$  is chosen specifically for the phase data. Figure 11 shows that the coefficients  $K_1$  and  $K_2$  are reasonably well correlated.

It would seem from figures 8 and 10 that the velocity distribution over a significant portion of the bed layer may be expressed as

$$\frac{u}{U_0} = K_1(y + Y) \cos(\omega t - K_2(y + Y) + \phi_0), \tag{4}$$

where  $\phi_0$  is the phase at  $y = -Y$  in figure 10 and  $\omega$  is equal to  $2\pi/T$ . This expression is similar to the limiting form of Stokes' (1851) solution for oscillatory flow over a flat bed (with axes fixed in the bed):

$$\frac{u}{U_0} \rightarrow \beta z \sqrt{2} \cos(\omega t - \frac{1}{2}\beta z + \frac{1}{4}\pi) \quad \text{as } z \rightarrow 0, \tag{5}$$

where  $\beta = (\omega/2\nu)^{\frac{1}{2}}$  and  $z$  is height measured up from the bed. However, it would seem

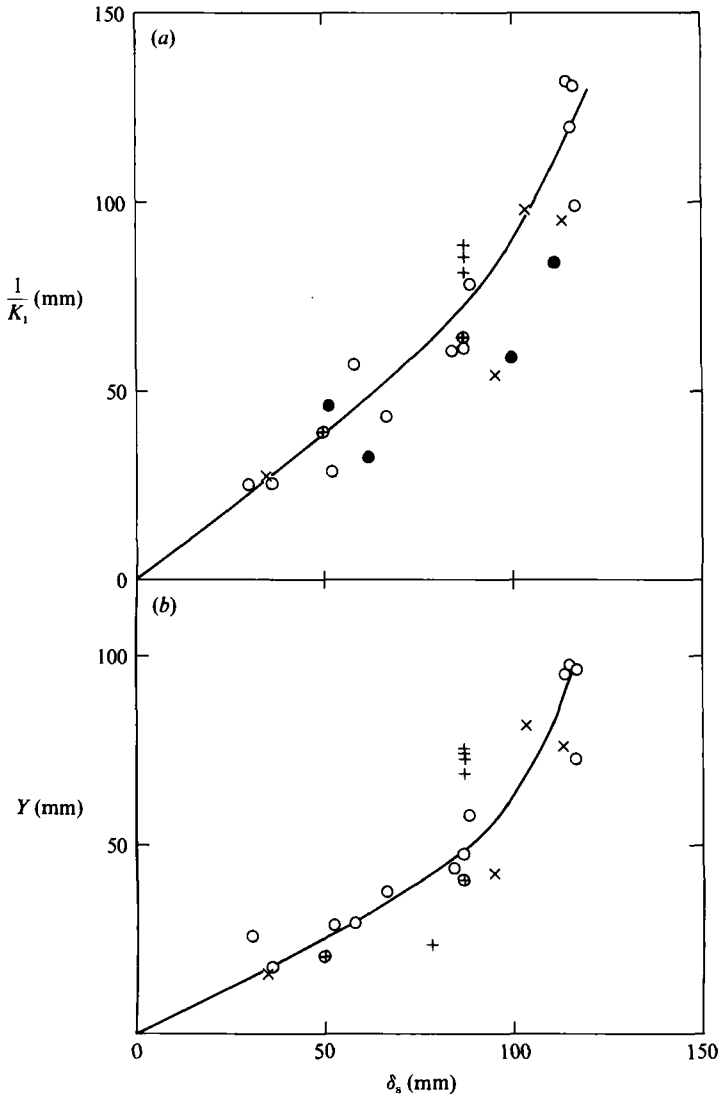


FIGURE 9. Variation of the parameters  $K_1$  and  $Y$  with  $\delta_s$ . ●, Ahilan (1985). Other symbols as in figure 7.

from figure 11 that the ratio  $K_1/K_2$  is generally less than unity rather than  $(8)^{1/2}$ . Also, the value of phase lead as  $y \rightarrow -Y$  in figure 10 is approximately  $71^\circ$  rather than  $45^\circ$  as suggested by (5).

### 8.2. Velocity measurements above the moving bed

One point of considerable interest is the extent to which the movement of the sediment affects the velocity distribution in the region above the bed. Sleath (1987) made velocity measurements over fixed beds in the same apparatus as was used for the present tests. He found that at large values of  $a/D$  the defect velocity distribution approached the well-known logarithmic law

$$\frac{\hat{u}_d}{\hat{u}_*} = -\frac{1}{0.4} \ln \frac{y_1}{y_{01}}, \quad (6)$$

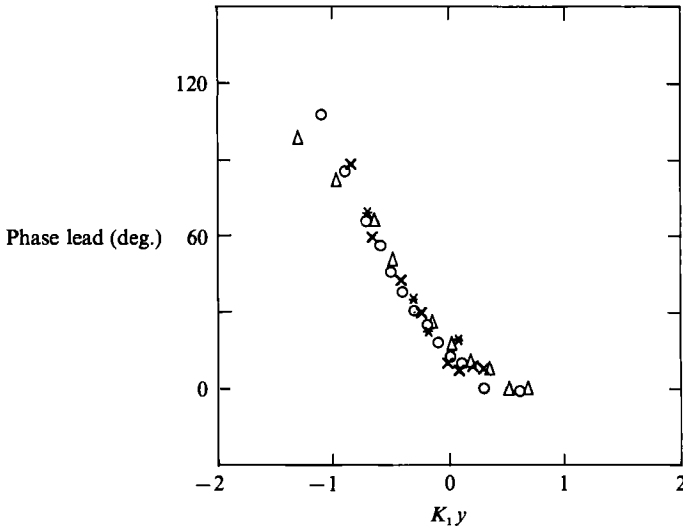


FIGURE 10. Variation of phase of horizontal velocity with height. Symbols shown in table 1.

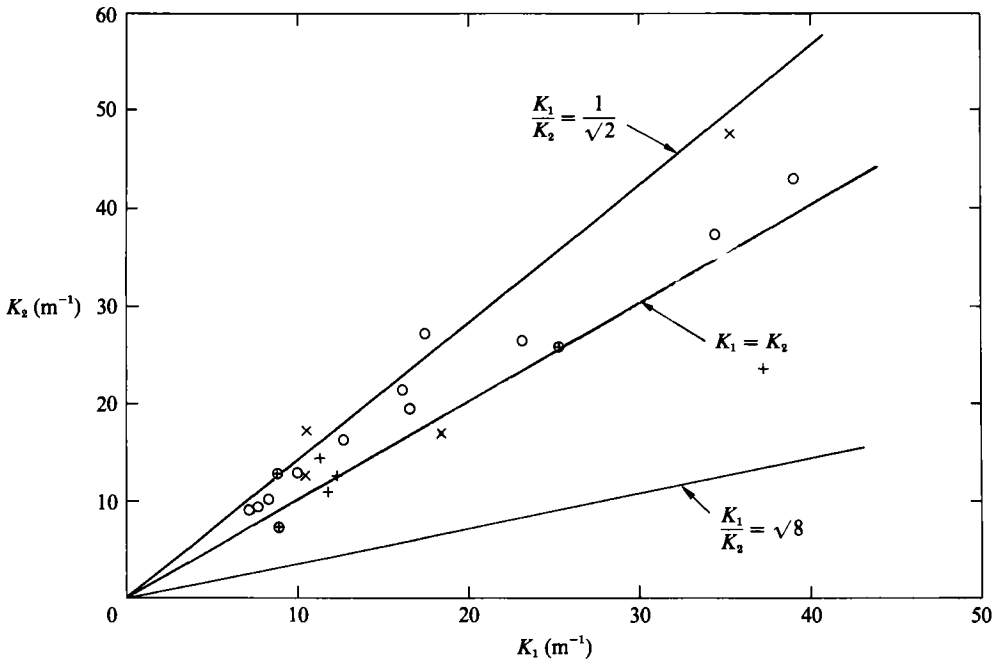


FIGURE 11. Variation of  $K_2$  with  $K_1$ .

where  $\hat{u}_*$  is the amplitude of the shear velocity at the bed,  $y_{01}$  is a constant and  $y_1$  is vertical height.

The main problem in the case of a moving bed is that it is not clear at what level to evaluate  $\hat{u}_*$  or where to take the origin for  $y_1$ . We will start by assuming that the appropriate value of  $\hat{u}_*$  is that at the initial bed level. The resulting values of shear velocity, calculated from the momentum integral, are listed in table 1. Figure 12 shows  $\hat{u}_d/\hat{u}_*$  plotted against  $y_1/y_{01}$ , for three tests with high values of  $a/D$ . We see

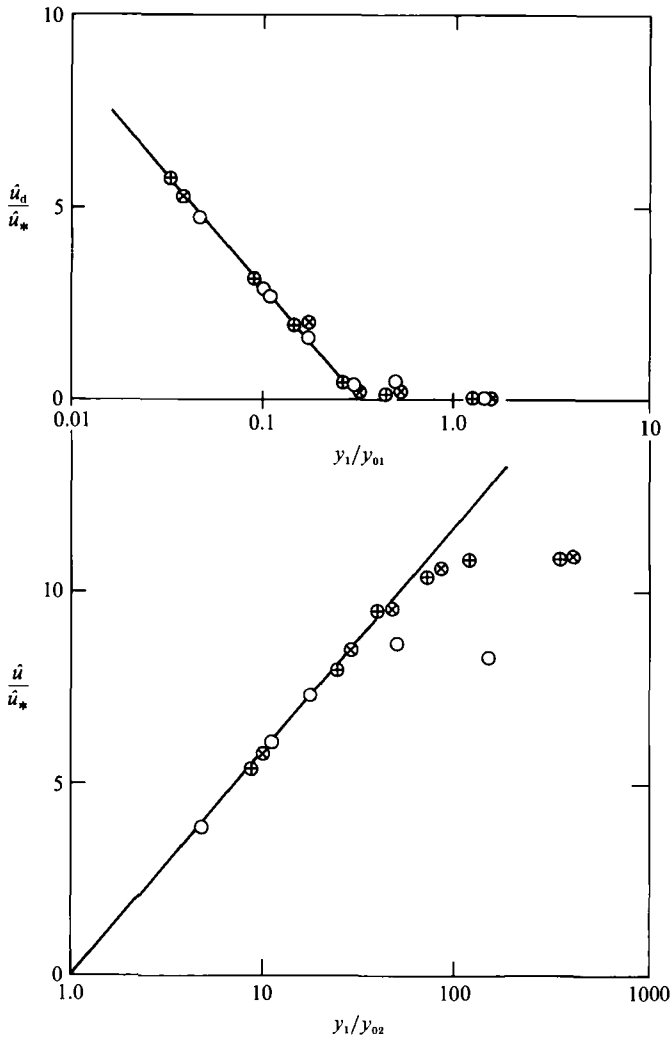


FIGURE 12. Fit of logarithmic velocity profiles to the experimental measurements. Symbols as in table 1.

that it is possible to match the experimental results to (6) over a certain range of heights provided the constant  $y_{01}$  and the origin of  $y_1$  are chosen so as to optimize the agreement. Figure 12 also shows how these results at high  $a/D$  compare with the corresponding logarithmic formula for the velocity amplitude  $\hat{u}$ :

$$\frac{\hat{u}}{\hat{u}_*} = \frac{1}{0.4} \ln \frac{y_1}{y_{02}}, \quad (7)$$

where  $y_{02}$  is another constant. We see that, once again, it is possible to match the experimental results to the logarithmic formula over a certain range of heights provided  $y_{02}$  is adjusted to optimize the agreement.

At smaller values of  $a/D$  the present experimental results show a tendency to deviate from (6) and (7) in the same way as was observed for fixed beds by Sleath (1987).

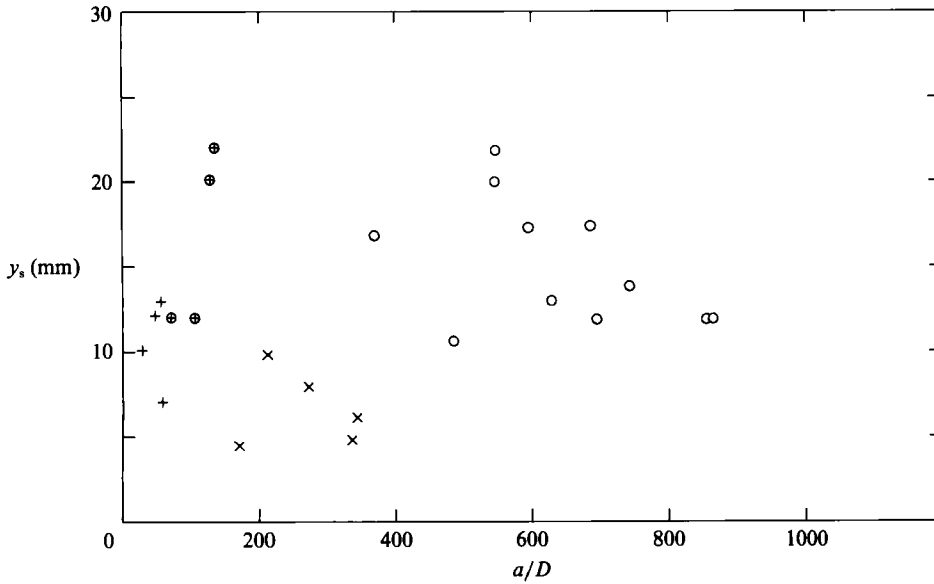


FIGURE 13. Distance of the origin of the logarithmic velocity profile below the initial bed level. Symbols as for figure 7.

Figure 13 shows how the distance  $y_s$  of the apparent origin of  $y_1$  beneath the initial bed level varies with  $a/D$ . There is no clear variation in  $y_s$  with either  $a/D$  or grain size. However, both sediments show smaller values of  $y_s$  at shorter periods. It may be that  $y_s$  scales with the Stokes thickness  $1/\beta$ .

For fixed beds the constants  $y_{01}$  and  $y_{02}$  in (6) and (7) have specific values. For a flat bed at zero pressure gradient  $y_{01}$  is equal to the thickness of the boundary layer and, if the bed is hydraulically rough,

$$y_{02} = \frac{k_s}{30.2}, \quad (8)$$

where  $k_s$  is the Nikuradse roughness length. In the present case we have no independent estimate of  $k_s$  and the value of boundary-layer thickness depends on what origin is chosen for velocity. Consequently, we cannot check the values of  $y_{01}$  and  $y_{02}$  obtained by fitting (6) and (7) to the experimental results. We can, however, carry out the reverse process and make use of (8) to estimate  $k_s$ . This gives the values of  $k_s/D$  shown in table 1 and plotted in figure 14. We see that  $k_s/D$  for these moving beds is very much larger than the values normally found with fixed beds. This is not unexpected since many investigators (e.g. Smith & McLean 1977; Grant & Madsen 1982) have drawn attention to the way in which bed roughness is increased by sediment transport.

The values of  $k_s/D$  in figure 14 show considerable scatter. Nevertheless, there does seem to be some agreement with the curve for  $k_s/D$  proposed by Wilson (1989). The results clearly do not agree with the curve of Grant & Madsen (1982). However, the experimental values of  $k_s/D$  are very sensitive to the assumed value of  $\hat{u}_*$ . If  $\hat{u}_*$  had been evaluated at, say, the still bed height the experimentally-determined values of  $k_s/D$  would have been very much larger. In figure 14,  $\psi'$  is the Shields parameter defined by (3).

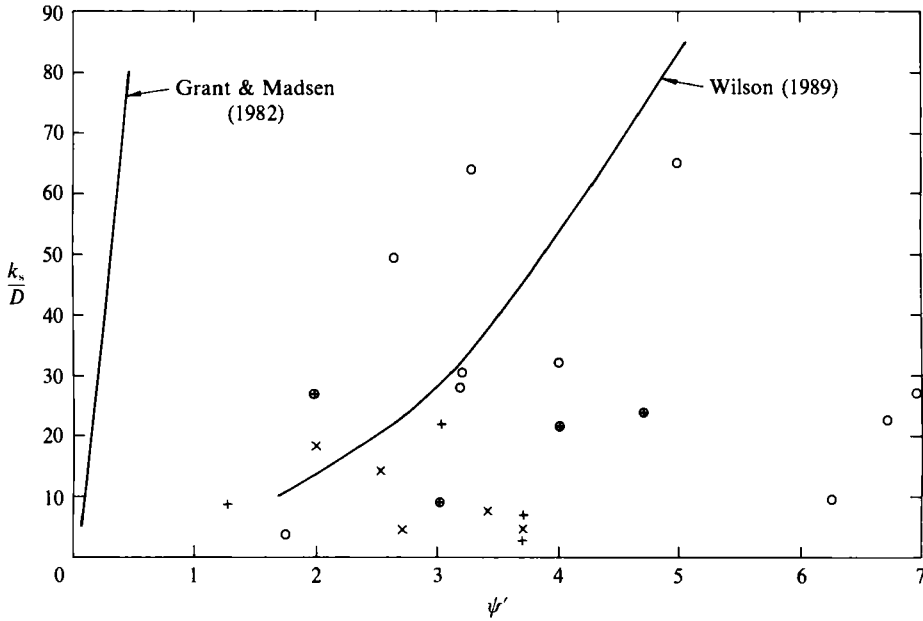


FIGURE 14. Variation of bed roughness length with Shields parameter. Symbols as for figure 7.

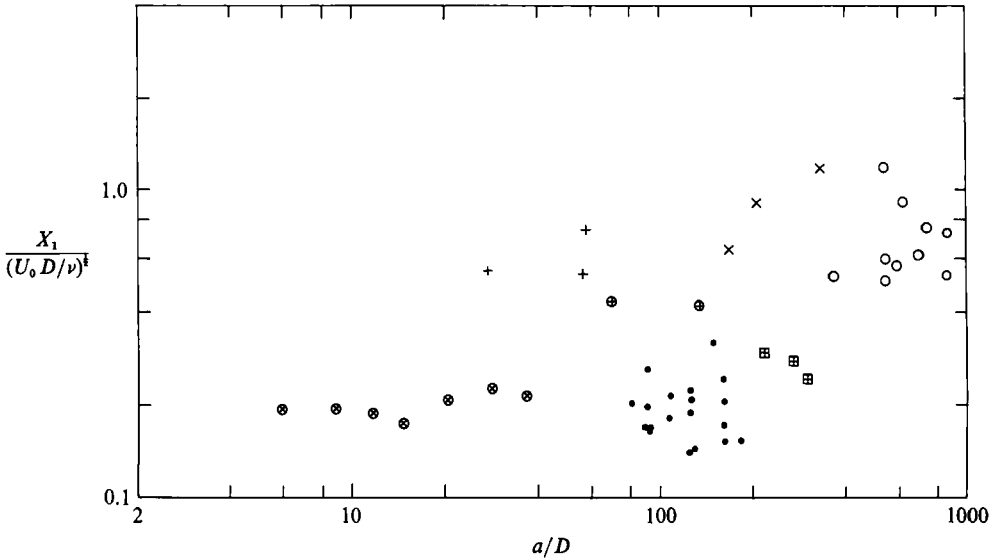


FIGURE 15. Comparison of the different values of the parameter  $X_1$ . Fixed beds:  $\otimes$ , Sleath (1982);  $\boxplus$ , Sleath (1987);  $\bullet$ , Kalkanis (1964). Mobile beds: Symbols as for figure 7.

Although a logarithmic curve can be fitted to the experimental velocity profiles, by appropriate choice of the constants  $y_{01}$  and  $y_{02}$  and the origin of  $y_1$ , the range of heights for which there is agreement is small. For example, for the 0.7 mm sediment, if the value of  $\hat{u}_*$  adopted is that at the initial bed level, the logarithmic layer only extends from the initial bed level to a height about 20 mm above. If  $\hat{u}_*$  is evaluated at some level below that, the range of heights for which the experimental results may

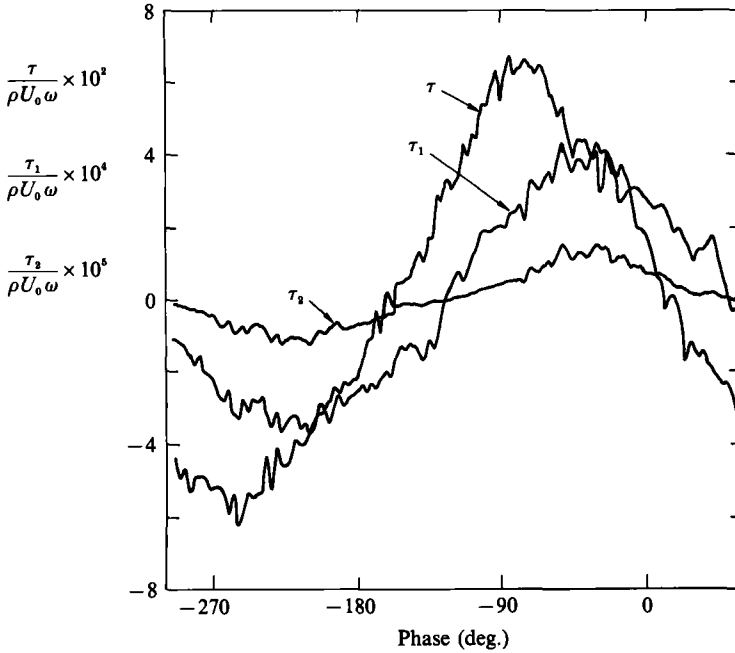


FIGURE 16. Variation of shear stress during the course of the cycle. Test 15 at 66.4 mm below the initial bed level.

be represented by a logarithmic curve is even less. It has been observed by several investigators that further out from the bed the velocity distribution is more closely described by an exponential expression. On the basis of fixed bed tests Sleath (1982) suggested

$$\hat{u}_d = \hat{u} \exp\left(-\frac{\beta y}{X_1}\right) \cos\left(\omega t - \frac{\beta y}{X_2} - \phi\right), \quad (9)$$

where  $X_1$ ,  $X_2$ ,  $\phi$  and  $\hat{u}$  are constants for any given test.

The velocity profiles for the present tests are similar in form to (9) but, as shown in figure 15, the actual values of  $X_1$  are larger for the movable bed tests than for the fixed bed tests. Larger values of  $X_1$  could be attributed to an increase in bed roughness, so this way of looking at the experimental results produces the same conclusion as that drawn from comparison with the log law profile.

### 8.3. Shear stress and apparent viscosity

Figure 16 shows a typical example of the way in which the shear stress varies with time at a fixed height within the moving bed of sediment. The shear stress was calculated from the momentum integral

$$\tau = \int_y^\infty \frac{\partial}{\partial t} (\rho u_\infty - \rho_m u) dy, \quad (10)$$

where  $u_\infty$  is the free-stream velocity and  $\rho_m$  is the density of the sediment/fluid mixture:

$$\rho_m = (1 - C)\rho + C\rho_s. \quad (11)$$

It should be emphasized that the calculation of shear stress from the momentum

integral is subject to error. This is because, at large distances from the bed, the integral represents the very small difference between large quantities. Experimental errors are consequently very much amplified. Many authors get round this problem by limiting the integration to heights above the bed which are small enough for errors in the defect velocity to be insignificant. We have adopted a similar procedure and have ignored defect velocities with amplitudes less than 5% of  $U_0$ . In addition, the integration above the initial bed level has been carried out on smooth curves fitted through the amplitude and phase measurements. Below the initial bed level the amplitude of the defect velocity is sufficiently large for the experimental records to be integrated directly. It is difficult to estimate the degree of uncertainty in these results because we have no independent measurement of shear stress. However, the calculated values of shear stress within the bed are relatively insensitive to the assumptions made for the region above the initial bed level. This is because, at large depths within the bed, the rate of change of the momentum of the fluid and sediment is small compared with the force due to the mean pressure gradient. Thus, at large depths within the bed the uncertainty is probably only a few per cent. On the other hand, at or above the initial bed level the uncertainty is much greater and the results for shear stress should consequently be treated with caution until confirmed by independent measurements.

Figure 16 also shows the shear stresses due to encounters between sediment particles calculated from the expressions suggested by Bagnold (1954). For the 'macro viscous' regime

$$\tau_1 = 2.2\lambda^{\frac{3}{2}}\mu \frac{\partial u}{\partial y}, \quad (12)$$

where  $\mu$  is dynamic viscosity of the fluid and  $\lambda$  is linear concentration of sediment

$$\lambda = \frac{1}{(C_*/C)^{\frac{1}{2}} - 1}, \quad (13)$$

with the limiting volumetric concentration for a stationary bed denoted by  $C_*$ . For the 'inertia' regime

$$\tau_2 = 0.013\rho_s(\lambda D)^2 \frac{\partial u}{\partial y} \left| \frac{\partial u}{\partial y} \right|. \quad (14)$$

Bagnold suggested that (12) should be used when  $\tau_1/\tau_2$  is greater than about 4.2, as in the present case, and (14) for  $\tau_1/\tau_2$  less than about 0.37.

It is clear from figure 16 that  $\tau_1$  is very much smaller than the shear stress  $\tau$  calculated from the momentum integral. The phase of  $\tau_1$  is also different from that of  $\tau$ .

The way in which the amplitude of the fluctuation in shear stress  $\hat{\tau}$  varies with height is shown in figure 17. Once again, the shear stress is calculated from the momentum integral. The dashed line in figure 17 corresponds to

$$\hat{\tau} = -\rho U_0 \omega y + \text{const.} \quad (15)$$

In the moving bed, the velocity  $u$  is close to zero. Under these circumstances (10) reduces to

$$\frac{\partial \tau}{\partial y} \doteq -\frac{\partial(\rho u_\infty)}{\partial t}, \quad (16)$$

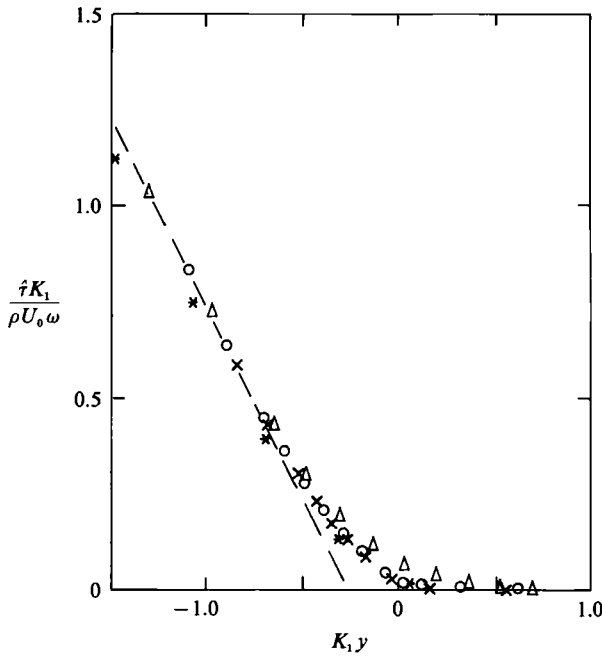


FIGURE 17. Variation of the amplitude of the shear stress with height above the initial bed level. ---, equation (15). Symbols as in table 1.

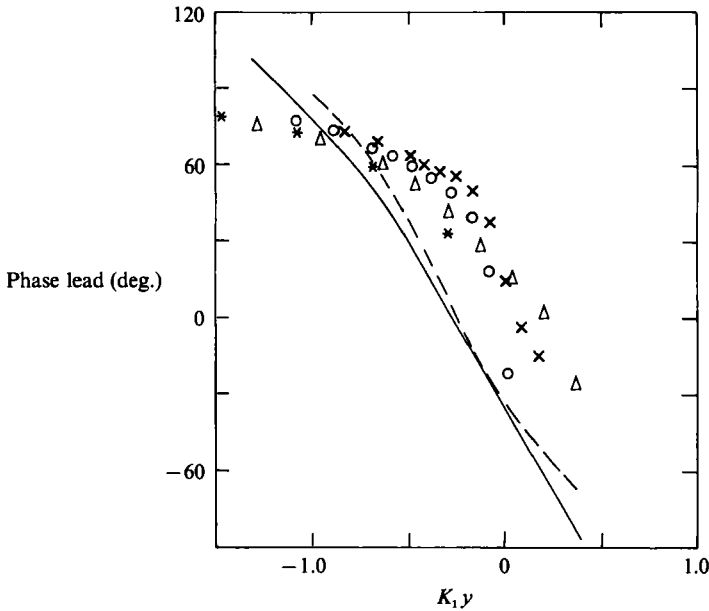


FIGURE 18. Variation of the phase of maximum shear stress with height above the initial bed level. —, phase of velocity gradient; ---, phase of Bagnold  $\tau_1$ . Symbols as in table 1.

which leads to (15). It would seem that near the bottom of the moving layer of sediment the shear stress is mainly determined by the free-stream pressure gradient. This conclusion is confirmed by figure 18 which shows that, within the moving bed, the phase of maximum shear stress is close to that of the free-stream pressure

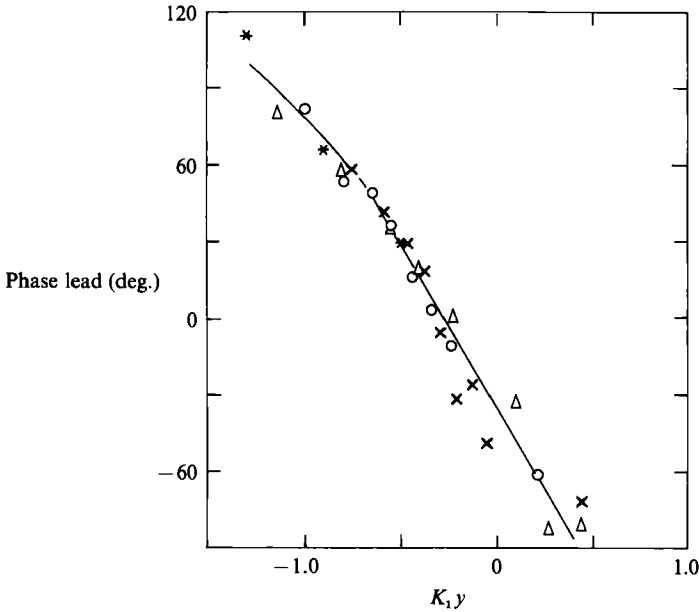


FIGURE 19. Variation with height of the phase of maximum velocity gradient. Symbols as in table 1.

gradient. As mentioned above, zero phase corresponds to maximum velocity in the free stream.

It might be expected that the phase of the maximum shear stress would be related to that of the velocity gradient  $\partial u/\partial y$ . Figure 19 shows how the velocity gradient varies with height for the same five tests as for figure 18. To facilitate comparison, the mean line through the measurements in figure 19 is also shown in figure 18. Although the two sets of experimental points have a similar trend there is a clear phase difference between the shear stress and the velocity gradient over most of the moving layer.

Figure 18 also shows Bagnold's shear stress  $\tau_1$  (for the conditions of Test 14). As would be expected from (12),  $\tau_1$  is nearly in phase with the velocity gradient. The slight difference between the two curves is due to the fact that  $\lambda$  also has a time-varying component. As already noted in connection with figure 16, the phase of the shear stress calculated from the momentum integral is significantly different from that of Bagnold's shear stress  $\tau_1$  over most of the depth of the moving bed. The curve for the amplitude of Bagnold's shear stress  $\tau_1$  does not appear on figure 17 because  $\tau_1$  is too small for the curve to be distinguished from the  $\tau = 0$  axis.

It ought to be mentioned that according to Bagnold  $\tau_1$  is not the total stress; when comparing with shear stress  $\tau$ , calculated from the momentum integral, we should add the intergranular fluid stress to  $\tau_1$  (or  $\tau_2$ ). Estimates of the intergranular fluid stress are uncertain but, in the present case, it is likely to be negligibly small except in the clearer fluid above the initial bed level. It would thus seem from figures 16, 17 and 18 that Bagnold's steady flow formulae for shear stress are not appropriate for oscillatory flow. A similar conclusion follows from the measurements of Bakker, Van Kesteren & Klomp (1990) in an oscillatory shear rig.

A parameter which appears in many sediment transport models is the value of the shear stress at the bed. It is clear from figure 17 that the value obtained depends on

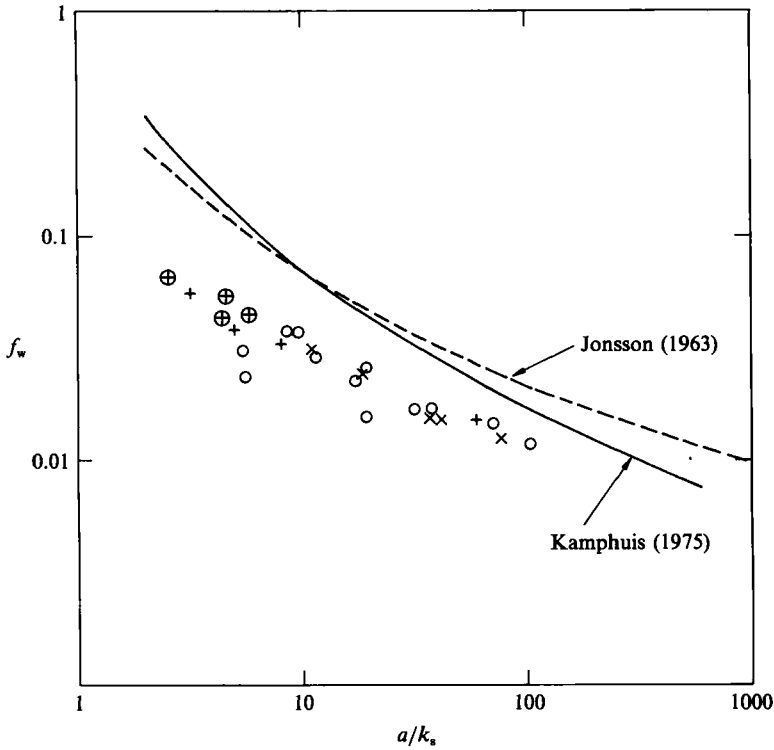


FIGURE 20. Comparison of measured friction factors with fixed bed curves. Symbols as for figure 7.

what one takes to be the bed level. Figure 20 shows how the value of friction factor based on the amplitude of the shear stress  $\hat{\tau}_0$  at the initial bed level compares with the curves of Jonsson (1963) and Kamphuis (1975) for fixed beds. Friction factor is defined here as

$$f_w = \frac{\hat{\tau}_0}{\frac{1}{2}\rho U_0^2}. \tag{17}$$

The value of  $k_s$  in figure 20 is the bed roughness length listed in table 1, obtained by fitting logarithmic curves to the velocity measurements.

We see that the experimentally determined values of friction factor all lie below the fixed-bed curves. This might seem surprising since we have already said that bed roughness, and hence  $f_w$ , are increased when the bed is mobile. The explanation is that although  $f_w$  is increased the value of  $a/k_s$  is decreased even more. If we had plotted  $f_w$  versus  $a/D$  the present values of  $f_w$  would all have lain above the fixed-bed results.

The results in figure 20 are based on the shear stress at the initial bed level. If we take a level deeper down in the bed we find larger values of  $f_w$ . However, the values of  $k_s$  obtained from a logarithmic curve fit are still larger, so that the experimental points end up even further from the fixed bed curves than those shown in figure 20. There appears to be no level within the moving bed for which the experimental points are in close agreement with the fixed-bed curves. This is hardly surprising in view of the fact, mentioned above, that a given logarithmic curve can only be fitted to the mobile-bed velocity measurements over a rather restricted range of heights.

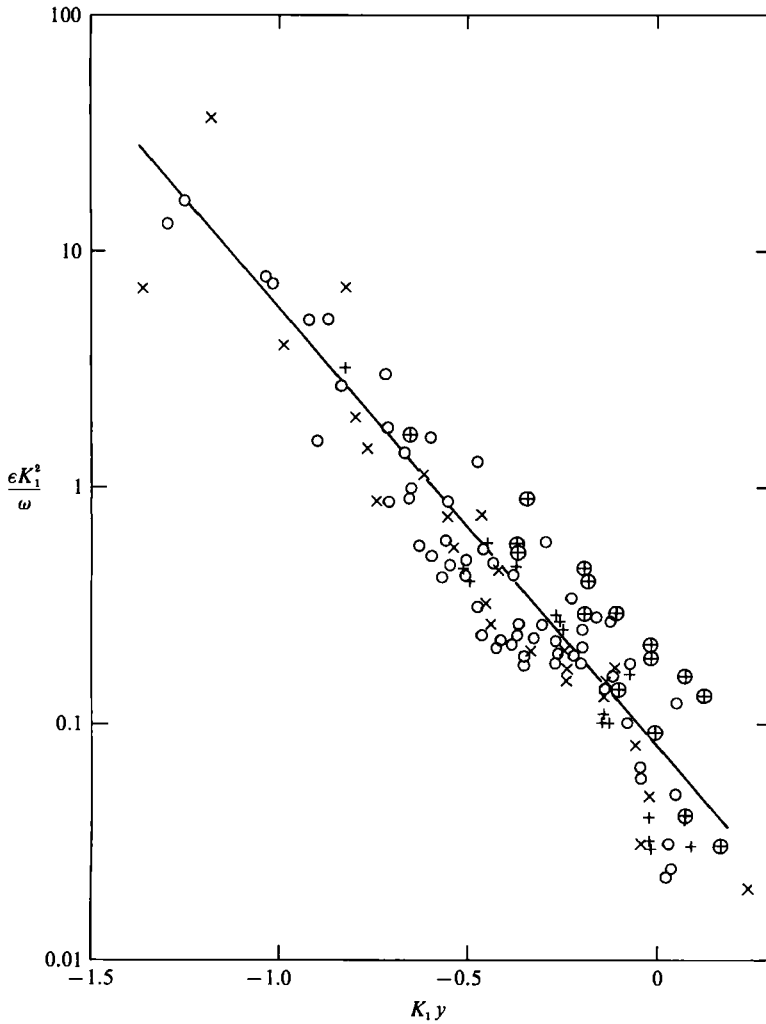


FIGURE 21. Variation of eddy viscosity with height above the initial bed level. Symbols as for figure 7.

Another point of interest for anyone attempting to model this sort of flow is the way in which the apparent viscosity  $\epsilon$ , defined by the expression

$$\tau = \rho \epsilon \frac{\partial u}{\partial y}, \quad (18)$$

varies within the moving bed. Figure 18 shows a phase difference between  $\tau$  and  $\partial u/\partial y$  over most of the moving bed. Under these circumstances, the apparent viscosity becomes infinite twice per cycle and experimental determination of the time-mean apparent viscosity becomes very inaccurate. In order to avoid this problem the apparent viscosity shown in figure 21 is the ratio of the amplitudes of  $\tau$  and  $\partial u/\partial y$  during the cycle.

The apparent viscosity and height are non-dimensionalized as shown in figure 21 because (4), (15) and figure 17 suggest that both  $(1/K_1 U_0) \partial u/\partial y$  and  $K_1 \hat{\tau}/\rho U_0 \omega$  are

functions of  $K_1 y$ . Although there is considerable scatter, the experimental points in figure 21 do seem to lie along a common curve. The straight line corresponds to

$$\frac{\epsilon K_1^2}{\omega} = 0.08 \exp(-4.25 K_1 y). \tag{19}$$

The origin of  $y$  in figure 21 is the initial bed level. Better agreement of the experimental results with (19) could have been obtained by fine tuning this origin.

Figure 21 only shows apparent viscosities within the moving bed. In the clear fluid above the bed the apparent viscosity rises again with height in the manner observed by, for example, Kemp & Simons (1982, 1983). The present measurements do not add anything new to the findings of previous investigators in this region of the flow.

### 9. Sediment concentration measurements

Figure 22 gives an example of how the concentration along a vertical varies with height and phase during the cycle. Within the moving bed layer the concentration remains high throughout the cycle whereas, above, the concentration falls off rapidly with height.

These trends are seen more clearly in figure 23 which shows the way in which the time-mean concentration varies with height. The straight line in figure 23 corresponds to the expression

$$\bar{C} = C_0 \exp(-y/l) \tag{20}$$

where  $l = 30D$  (the value suggested by Nielsen (1986) for sheet flow) and  $C_0$  is a constant. Although the experimental results show considerable scatter their general trend appears to be in reasonable agreement with this equation in the region above the moving bed.

The concentration  $C_0$  at  $y = 0$  is an important parameter for those attempting to estimate quantities of sediment moved in suspension by wave action. Figure 24 shows how the value of  $C_0$  depends on the Shields parameter  $\psi'$  defined by (3). The straight line in this figure is the expression proposed by Nielsen (1986) for sheet flow:

$$C_0 = 0.005\psi'^3. \tag{21}$$

Although the experimental points show no discernible trend by themselves they do lie remarkably close to Nielsen's curve when it is borne in mind that the values of  $C_0$  on which it is based were much smaller than those in the present tests.

It will be seen from figure 22 that the concentration fluctuates during the course of the cycle. The temporal variation in concentration at a given height is approximately sinusoidal with frequency twice that of the velocity. An example of the concentration record is given in figure 25. Figures 26 and 27 show how the amplitude and phase of the fluctuating component of concentration vary with height. The same origin for height  $y$  and the same scaling factor  $K_1$  have been used as for the velocity distributions shown in figures 8 and 10. Although there is more experimental scatter than for the velocities the trends are reasonably clear. The amplitude  $\hat{C}$  of the fluctuation in concentration is maximum at about the initial bed level and falls off steadily both above and below that point. For the present range of measurements, the phase lead of maximum concentration also shows a turning point (this time a minimum) at about the initial bed level. Within the moving bed the phase of maximum concentration appears to be closely linked to that of the velocity gradient. The mean curve through the experimental points in figure 19 is reproduced

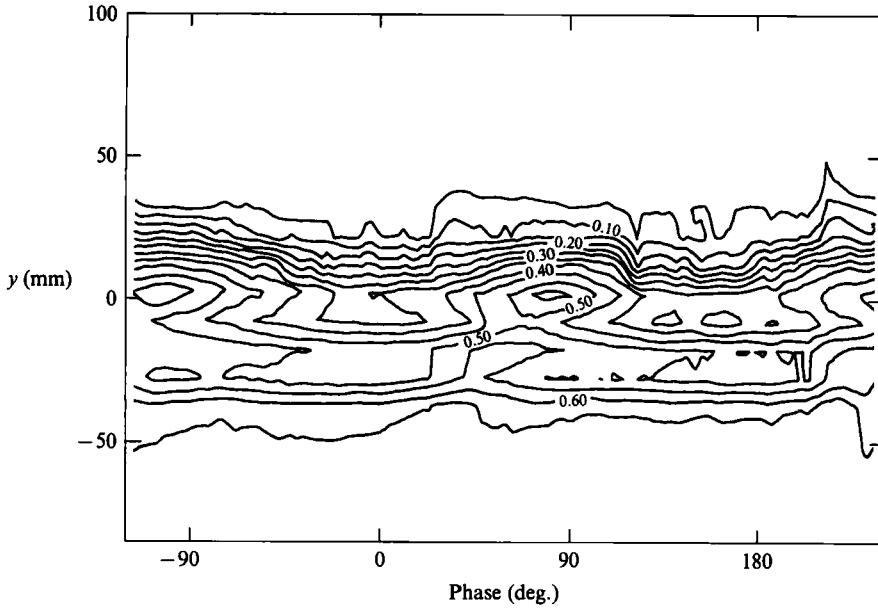


FIGURE 22. Variation of concentration with height and time at a fixed vertical section. Numbers on profiles represent volumetric concentration of sediment in  $\text{m}^3/\text{m}^3$ . Test 12.

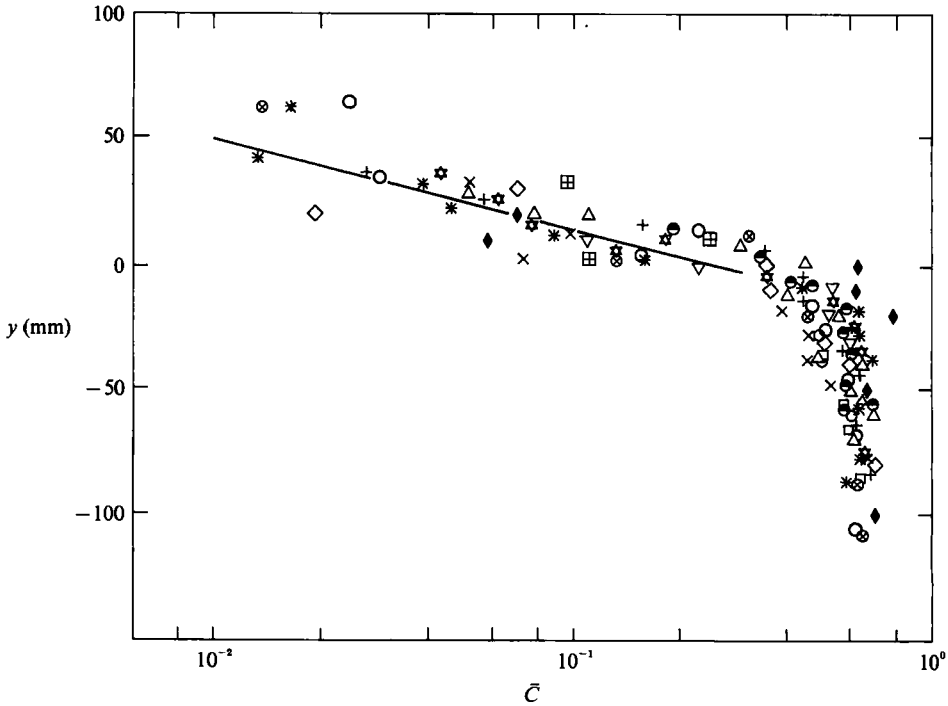


FIGURE 23. Variation of time-mean concentration with height above the initial bed level. Symbols as in table 1.

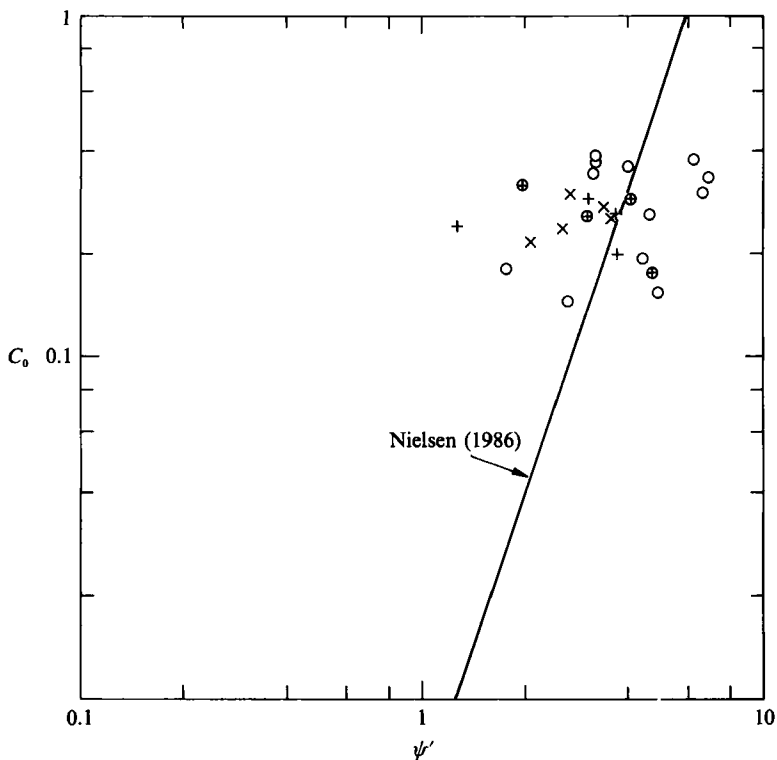


FIGURE 24. Time-mean concentrations at the initial bed level. Symbols as for figure 7.

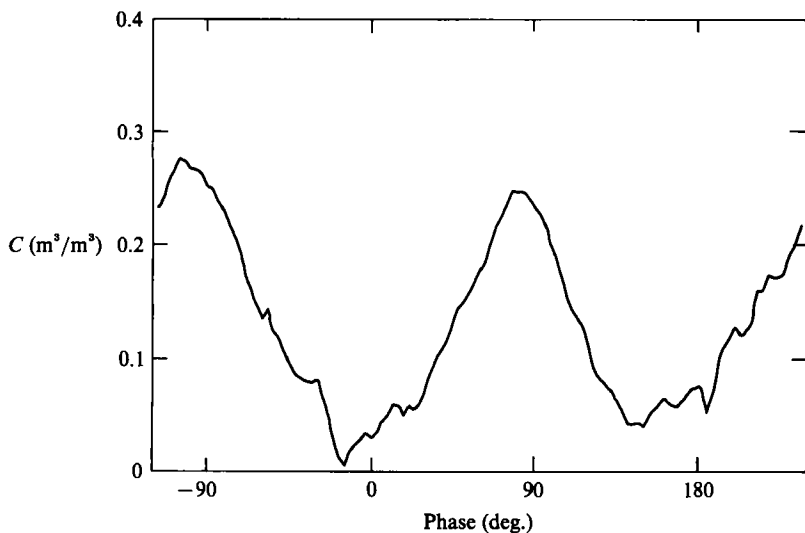


FIGURE 25. Example of variation in concentration with time. Test 12 at a height of 3.7 mm above the initial bed level.

in figure 27. We see that the phase of maximum concentration within the moving-bed layer is almost exactly in quadrature with that of the velocity gradient. In other words, maximum concentration coincides closely with zero velocity gradient, which is what one might expect. However, above the moving bed the trend is different.

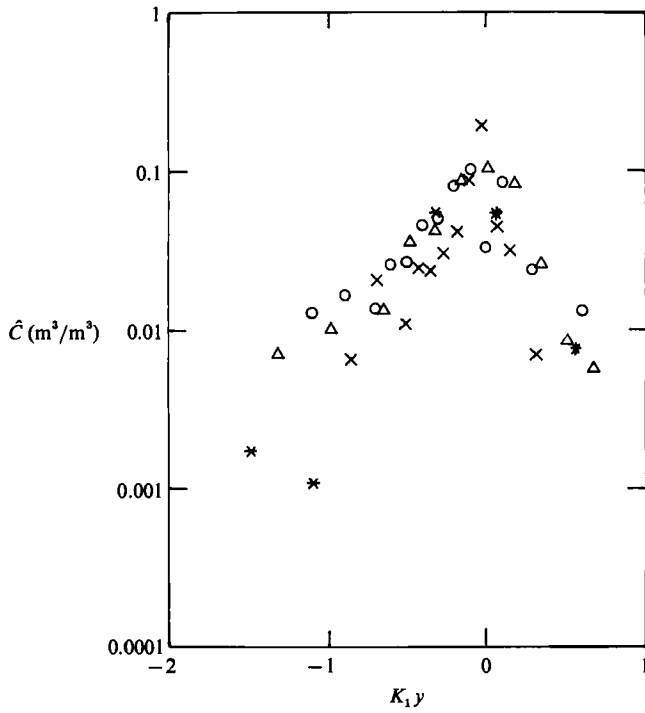


FIGURE 26. Variation with height of the amplitude of the fluctuation in concentration. Symbols as in table 1.

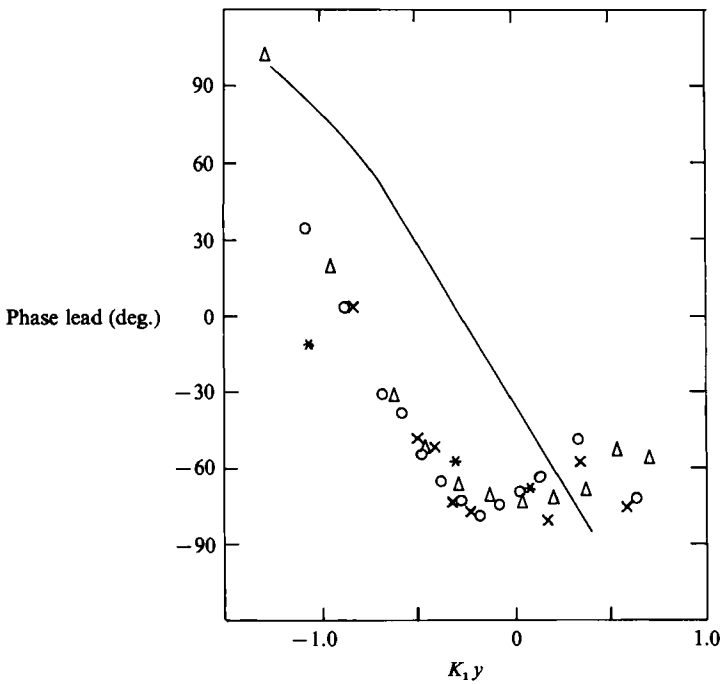


FIGURE 27. Variation with height of the phase of maximum concentration. —, phase of velocity gradient. Symbols as in table 1.

While the phase lead of velocity gradient continues to decrease with height, that of maximum concentration increases. There are several mechanisms which might account for this change in trend. An important factor is likely to be the dilatation of the bed owing to movement of the sediment. By itself, this mechanism would produce maximum concentration, at any given point above the initial bed level, when the vertically averaged concentration below was minimum. However, even above the initial bed level, the velocity gradient will also have a significant effect on the fluctuation in concentration. Finally, upward entrainment of sediment by fluid turbulence or by vortices associated with ripples is likely to be important in this region above the initial bed level and might, consequently, contribute to the observed change in trend of the phase shift.

Another way of investigating the fluctuation in concentration with time at any given point is to compare the maximum concentration  $C_{\max}$  and the minimum  $C_{\min}$  with the time-mean value  $\bar{C}$ . Homma, Horikawa & Kajima (1965) found, for suspended sediment above a rippled bed,

$$C_{\max} = 1.9\bar{C}, \tag{22}$$

$$C_{\min} = 0.59\bar{C}. \tag{23}$$

Figures 28 and 29 show the results for the 0.7 mm sediment with  $T \doteq 4.5$  s. The results for the other tests are very similar. We see that at very low concentrations, i.e. above the initial bed level, the present results show reasonable agreement with Homma *et al.*'s expression but that deeper down in the bed the measurements tend progressively towards the curve.

$$C_{\max} = C_{\min} = \bar{C}, \tag{24}$$

as might be expected.

## 10. Conclusions

(i) The measured velocity profile may be divided into three regions: a central region in which velocity amplitude and phase vary almost linearly with height and transition regions to the free stream above and the stationary bed below. At high sediment transport rates the central region covers almost the entire depth of the moving bed but under less severe flow conditions the transition regions are relatively more important.

(ii) The movement of the bed has a significant effect on the velocity distribution in the fluid above. Bed roughness length is increased and the amplitude of the velocity falls off more slowly than for a fixed bed under equivalent flow conditions. Although it is possible to fit logarithmic curves to segments of the velocity profile by suitable choice of the disposable coefficients, the agreement is only good over a relatively small part of the boundary layer.

(iii) Shear stress and apparent viscosity rise steadily with depth below the surface of the moving bed. Lower down, the variation of shear stress with height is almost linear, as would be expected if pressure gradient were the dominant effect.

(iv) The concentration measurements are in good agreement with the results of other investigators in the region above the moving bed. Within the bed the time-mean concentration rises uniformly with depth towards a limiting value for the stationary bed. Superimposed on the time-mean concentration there is a fluctuation in concentration at twice the frequency of the fundamental oscillation. The

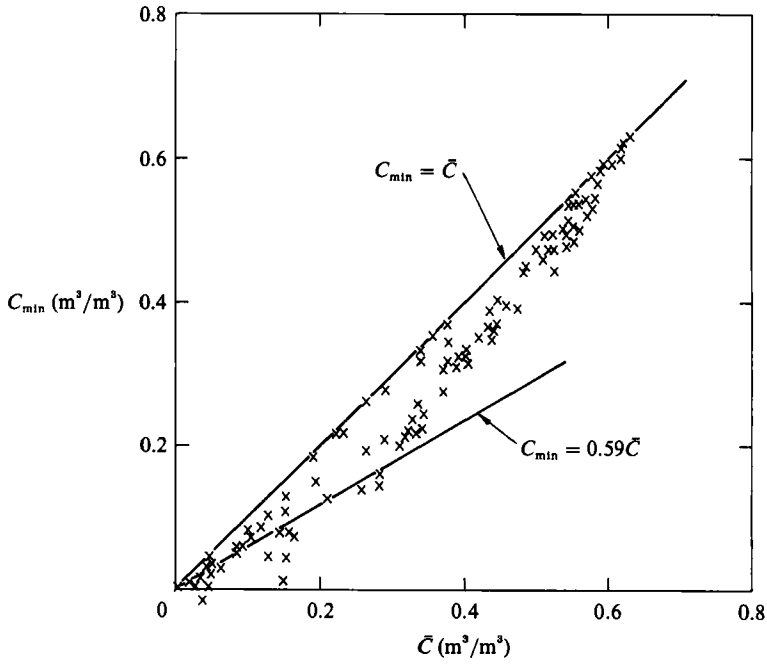


FIGURE 28. Variation of minimum concentration with time-mean concentration. Tests 5-18.

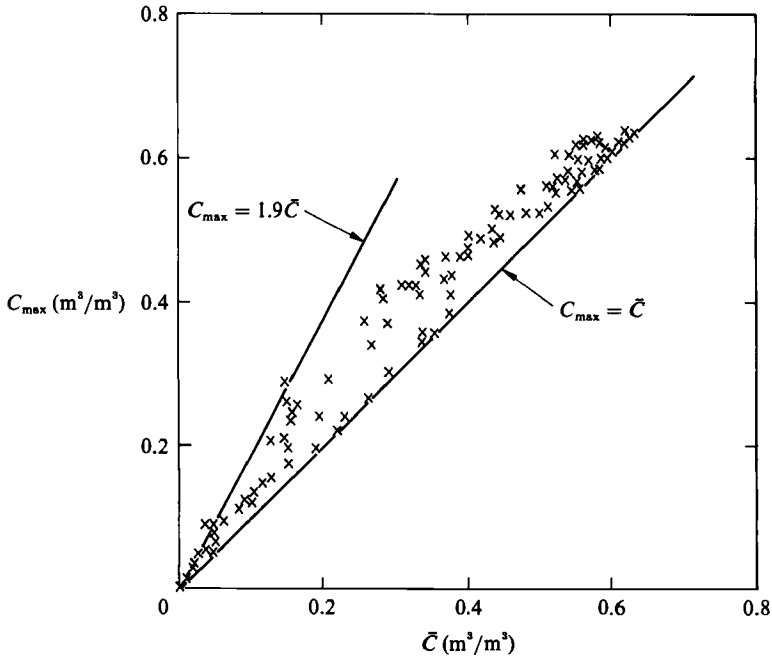


FIGURE 29. Variation of maximum concentration with time-mean concentration. Tests 5-18.

amplitude of this fluctuation falls steadily both above and below the initial bed level. Within the moving bed its phase is close to that of zero velocity gradient.

#### REFERENCES

- ABOU-SEIDA, M. M. 1965 Bed load function due to wave action. *Hydraul. Engng Lab. Rep. HEL* 2-11, University of California, Berkeley, 78 pp.
- AHILAN, R. V. 1985 Flow of cohesionless grains in oscillatory fluids. PhD thesis, University of Cambridge, 191 pp.
- AHILAN, R. V. & SLEATH, J. F. A. 1987 Sediment transport in oscillatory flow over flat beds. *J. Hydraul. Div. ASCE* **113** (3), 308-322.
- BAGNOLD, R. A. 1954 Experiments on a gravity-free dispersion of large solid spheres in a Newtonian fluid under shear. *Proc. R. Soc. Lond. A* **225**, 49-63.
- BAKKER, W. T., VAN KESTEREN, W. G. M. & KLOMP, W. H. G. 1990 Grain-fluid interaction in Couette flow. In *Proc. 22nd Intl Conf. Coastal Engng.* Delft, pp. 2696-2709.
- CHUA, S. K., CLEAVER, J. W. & MILLWARD, A. 1986 The measurement of salt concentration in a plume using a conductivity probe. *J. Hydraul. Res.* **25** (3), 171-178.
- DICK, J. E. 1989 Sediment transport in oscillatory flow. PhD thesis, University of Cambridge, 169 pp.
- DINGLER, J. R. & INMAN, D. L. 1976 Wave formed ripples in nearshore sands. In *Proc. 15th Conf. Coastal Engng.*, pp. 2109-2126.
- DURAO, D. F. G., ADRIAN, R. J., DURST, F., MISHINA, H. & WHITELAW, J. H. (eds) 1982 *International Symposium on Applications of Laser-Doppler Anemometry to Fluid Mechanics.* Lisbon.
- DU TOIT, C. G. & SLEATH, J. F. A. 1981 Velocity measurements close to rippled beds in oscillatory flow. *J. Fluid Mech.* **112**, 71-96.
- GIBSON, C. H. & SCHWARZ, W. H. 1963 Detection of conductivity fluctuations in a turbulent flow field. *J. Fluid Mech.* **16**, 357-364.
- GRANT, W. D. & MADSEN, O. S. 1982 Moveable bed roughness in unsteady oscillatory flow. *J. Geophys. Res.* **87** (C1), 469-481.
- HANES, D. M. & INMAN, D. L. 1985 Observations of rapidly flowing granular-fluid materials. *J. Fluid Mech.* **150**, 357-380.
- HOMMA, M., HORIKAWA, K. & KAJIMA, R. 1965 A study on suspended sediment due to wave action. *Coastal Engng Japan* **8**, 85-103.
- HORIKAWA, K., WATANABE, A. & KATORI, S. 1982 Sediment transport under sheet flow conditions. *Proc. 18th Conf. Coastal Engng.*, vol. 2, pp. 1335-1352.
- JONSSON, I. G. 1963 Measurements in the turbulent wave boundary layer. *Proc. 10th IAHR Congress, London*, pp. 85-92.
- KALKANIS, G. 1964 Transportation of bed material due to wave action. *Tech. Memo. 2*, US Army Corps of Engineers, Coastal Engng Res. Center.
- KAMPHUIS, J. W. 1975 Friction factors under oscillatory waves. *J. Waterways, Port, Coastal and Ocean Engng Div. ASCE* **101** (WW2), 135-144.
- KEMP, P. H. & SIMONS, R. R. 1982 The interaction between waves and a turbulent current: waves propagating with the current. *J. Fluid Mech.* **116**, 227-250.
- KEMP, P. H. & SIMONS, R. R. 1983 The interaction of waves and a turbulent current: waves propagating against the current. *J. Fluid Mech.* **130**, 73-89.
- KRUMBEIN, W. C. & MONK, G. D. 1942 Permeability as a function of the size parameters of unconsolidated sand. *Am. Inst. of Mining and Met. Engng Tech. Pub.* 1492.
- LANDAUER, R. 1952 The electrical resistance of binary metallic mixtures. *J. Appl. Phys.* **23** (7), 779-784.
- MANOHAR, M. 1955 Mechanics of bottom sediment movement due to wave action. *Tech. Memo. 75*, US Army Corps of Engineers, Beach Erosion Board.
- NIELSEN, P. 1984 On the motion of suspended sand particles. *J. Geophys. Res.* **89** (C1), 616-626.
- NIELSEN, P. 1986 Suspended sediment concentrations under waves. *Coastal Engng* **10**, 23-31.

- SAVAGE, S. B. & MCKEOWN, S. 1983 Shear stresses developed during rapid shear of concentrated suspensions of large spherical particles between concentric cylinders. *J. Fluid Mech.* **127**, 453–472.
- SAWAMOTO, M. & YAMASHITA, T. 1986 Sediment transport rate due to wave action. *J. Hydrosci. Hydraul. Engng* **4** (1), 1–15.
- SLEATH, J. F. A. 1978 Measurements of bed load in oscillatory flow. *J. Waterways, Port, Coastal and Ocean Div. ASCE* **104** (WW3), 291–307.
- SLEATH, J. F. A. 1982 The effect of jet formation on the velocity distribution in oscillatory flow over flat beds of sand or gravel. *Coastal Engng* **6**, 151–177.
- SLEATH, J. F. A. 1987 Turbulent oscillatory flow over rough beds. *J. Fluid Mech.* **182**, 369–409.
- SMITH, J. D. & MCLEAN, S. R. 1977 Boundary layer adjustments to bottom topography and suspended sediment. In *Bottom Turbulence* (ed. J. C. J. Nihoul), pp. 123–151. Elsevier.
- STOKES, G. G. 1851 On the effect of the internal friction of fluids on the motion of pendulums. *Trans. Camb. Phil. Soc.* **9**, 20–21.
- WILSON, K. C. 1989 Friction of wave-induced sheet flow. *Coastal Engng* **12**, 371–379.